Study on SPECT/CT Imaging Features and Related Pathology of Cystic Generation of the Talus

Qitao Song
Tianjin Hospital
Xiantie Zeng
Tianjin Hospital
Haijing Huang
Tianjin Hospital
Lei Long
Tianjin Hospital
Jin Xu
Tianjin Hospital
Shuangshuang Cui
Tianjin Hospital
Zhonghai Li (lizhonghaispine@126.com)
First Affiliated Hospital of Dalian Medical University
Xinlong Ma
Tianjin Hospital

Research Article

Keywords: Talus, Cystic generation, SPECT/CT, Diagnosis, Treatment

Posted Date: February 1st, 2022

DOI: https://doi.org/10.21203/rs.3.rs-1304398/v1

Abstract

Objective: To explore the imaging features of three-phase bone and SPECT/CT images of cystic lesions on the talus.

Methods: A total of 189 patients with suspected chronic pain in the ankle joint of the talus cystic degeneration were enrolled in this retrospective study, who underwent 99mTc-MDP three-phase bone imaging and delayed SPECT/CT scans in our hospital. The location, range of involvement, classification, CT value, and radioactivity uptake of the sclerosis of cystic lesions on the talus, and the continuity of articular surface were observed. Comparisons were analyzed with the pathological results.

Results: Totally, 83% (157/189) of the talar cysts were located to the medial fornix, most of which involved the anterior middle part (43.27%), and the larger cysts involved the posterior part (9.6%). 63% (119/189) of the patients were type I, and 37% (70/189) of the patients were type II. The articular surface of the medial dome of the talus of all of the patients was intact, and the subchondral bony articular surface of 88% (166/189) patients was rough. The coincidence rate of the location, type, range of involvement of cystic lesions with pathological results was 87.83% (166/189). The CT value of cystic lesions was 45 15Hu (30-60Hu). The percentage of pathological chondrogenesis in the high CT value ≥ 50Hu (19/70) group and the low CT value < 50Hu (51/70) group were 89.47% (17/19) and 29.14% (15/51) (c2=20.12, P□0.001), respectively. The T/B ratio of the radioactivity uptake area of the talus vault was 2.0±0.5(1.5-2.5). The percentage of pathological new trabecular bones in T/B ratio≥2.0 (157/189) group and T/B ratio□2.0 (32/189) group (c2=45.08□P□0.001) were 82.80% (130/157) and 25.00% (8/32), respectively.

Conclusions: Three-phase bone imaging could identify the damage of the talus caused by cystic degeneration, and delayed SPECT/CT images have certain advantages in display the location, range of involvement, classification, and repair of cystic lesions of the talus.

Background

Osteochondral lesions of the talus (OLT) are a common orthopaediccondition. It is a talar lesion due to multiple causes, characterized by cartilage damage, loosening, exfoliation, or subchondral osteonecrosis and formation of free osteochondral bodies. It was first described by Monro in 1856 as one of the causes of chronic pain in the ankle joint. In 1959, Berndt and Harty classified OLT into four types [1]: type 1 for simple compression injury, type 2 for partial cartilage fracture, type 3 for complete separation of cartilage fracture fragments without displacement, and type 4 for the displacement of fracture fragments. In 1993, Richard reported that the application of SPECT and CT to the same patients revealed that radiolucent defects and bone defects could be observed in the talus in 77% of patients. Berndt's classification did not include this type of condition. He added type 5, an area of intraosseous x-ray hypodense defect, to Berndt's classification [2]. This image is extremely similar to the imaging of ischemic necrosis of the talus complicated by a talar neck fracture, but these are two very different lesions. When abnormalities in bone

density (or signal) of the talar body (apex of the fornix) with concomitant bone defects and cystic changes are found on X-ray, CT, and MRI, it is undoubtedly important to accurately determine the nature of the lesion and make a correct diagnosis for the treatment and prognosis of the patient.

With the continuous advances in medical imaging equipment, especially the implementation of SPECT/CT, the rate of diagnosis of trauma and disease in the field of orthopedics has increased dramatically, and the understanding of the nature of injury and disease has been elevated to a new level. In the case of osteochondral injuries of the talus, according to a multicenter study in Canada, the center diagnosed 13 patients in five years from 1981-1986, while in the next five years (1987-1992), the same group diagnosed 79 diseases, a sixfold increase, and proposed new classifications [2].

To identify those two different lesions, this study was conducted to evaluate the blood supply and bone metabolism in osteochondral injury cystic lesions of the talus by using SPECT/CT triphasic bone imaging and 16-row CT fusion images on the same machine in patients with chronic ankle pain without fracture-dislocation. To make a preliminary analysis of the characteristics and causes of osteochondral injury cystic lesions of the talus in comparison with the pathological findings of surgical specimens.

Methods

Participants

A total of 189 patients with chronic pain in the ankle joint clinically suspected of talar cystic degeneration were enrolled from our hospital, including 135 males and 54 females, with an age range of 23-66 years and a mean age of 41 years (Table 1). Inclusion criteria: (1) history of different degrees of ankle sprains; (2) clinical manifestation of chronic intermittent ankle pain combined with recurrent mild ankle swelling, weakness, and stiffness; (3) VAS (visual analogue scale, 0-10) score ≤3, and unaffected sleep at night; (4) uneven subchondral bone density in the medial (and in a few cases lateral) talar domes by X-ray plain radiographs, and unclear bony articular surface due to joint overlap and insignificantly narrowed joint space; (5) SPECT/CT three-phase bone scan. Exclusion criteria: (i) patients with talar fractures; (ii) patients with a history of long-term heavy alcohol consumption and hormone therapy. All patients underwent surgical circumferential drilling of the damaged cystic area of the talus in our hospital and were filled with autologous osteochondral column mosaic graft. Intraoperative specimens were sent to pathology for definitive diagnosis.All participants had given informed consent to use their information for research purposes.

^{99m}Tc-MDP SPECT/CT scans

A Discovery NM670 SPECT/CT machine (GE Healthcare, USA) equipped with a low-energy, high-resolution parallel-hole collimator was used. The patientswereinjected with the 99mTc-methyl diphosphonate (99mTc-MDP) 740 MBq (volume <1 ml) via the elbow vein. 99mTc-MDP was produced by HTA Co. with a radiochemical purity of morethan 95%.

Anterior and posterior planar images of the perfusion phase, blood pool phase, delayed phase, andimages of the delayed phase of the ankle were acquired bilaterally. Three-phases acquisition parameters were as follows: energy peak 140 KeV, window width 20%, matrix 128×128, Zoom 1.25. Perfusion phase(Figure 1): immediately after intravenous injection of the imaging agent, continuous acquisition at 2s/frame for 60 seconds. The arterial blood flow was observed to determine whether local "congestion" or "ischemia." Blood pool phase(Figure 2): after the end of the perfusion phase acquisition, 1 min/frame, 10 minutes of continuous acquisition. The soft tissue venous blood flow was observed to determine whether it was local "bruising." Delayed phase(Figure 3): 2 hours after the injection of the imaging agent, the acquisition count reached 1×105kcts. The tracer in the soft tissue faded, and the tracer in the bone showed clearly, which could reflect the bone metabolic condition. CT acquisition parameters were as follows: 120 kV tube voltage, 150 mA, layer thickness 10 mm, pitch 1.0.

Image analysis

In order to further clarify the extent of "ischemia" and "necrosis" in the damaged talus, we used 99mTc-MDP SPECT/CT bone triple-phase scanning and simultaneous fusion imaging. The first was to clarify whether the inhomogeneous bone density area shown by X-ray coincides with the abnormal tracer uptake area. The second was to visually observe whether there was a blank of tracer distribution or abnormal concentration in the cystic area of the talus. If the local tomographic image was "white," this area would be ischemic. Otherwise, the local tomographic image was "black", reflecting abundant blood flow and high bone metabolism in the lesion area.

The SPECT/CT images were fused and analyzed using the Xeleris workstation (GE Healthcare, USA): Observe the location of the talar fornix lesion and record it on the Elias nine-pattern [3] (Figure 4); Clarify the extent of involvement of the talar cystic lesion; Classify the lesion according to the extent of the cystic lesion and the number of lesions. Type I: It consisted of several independent and staggered bursae under the articular surface of the fornix, which were separated and surrounded by a bony sclerotic zone(Figure 5). Type II: it was developed from type I, containing a large thin-walled spherical cystic lesion. The cystic lesion was approximately 10-15 mm in diameter, with thin-walled sclerosis visible at the edges and a large cyst located deep, often below the small cyst, anterior to the middle of the medial fornix, connected to the small cyst or extending upward to the articular surface through a narrow channel (Figure 6). Type II was more symptomatic and had a poorer prognosis; The CT of the cystic lesion was measured to indirectly reflect the tissue composition within the lesion area [4-6]; The bone continuity of the articular surface above the cystic area was observed from sagittal, coronal, and transverse views in all directions; The hematologic metabolism of the sclerotic zone was observed, and a non-uniformly thickened sclerotic zone was formed by the deposition of new bone minerals around the subchondral bone cystic lesion, and semi-quantitative analysis was used to measure the ratio of the degree of concentration of the affected side to the healthy side concentration zone (T/B ratio).

Pathological analysis

The specimens taken intraoperatively were processed to observe the morphology and the visible type of tissue. Then analyses were performed by microscopic observation. The gross specimen showed focal wear thinning of the cartilage in the talar fornix with visible fractures and partial subchondral bone defects. Mucus-like material remaining was found in the larger cystic lesions (Figure 7). Microscopically, some of the bone traps were empty, osteoblasts were missing, fibroblasts were proliferating, collagen fibers were abundant, inflammatory cells were aggregating, and fibroblastic tissue was visible growing in between the necrotic bone trabeculae (Figure 8). Folded and tortuous fibrous cyst walls were seen in intact specimens, and scattered bone-like stroma was visible between the hyperplastic granulation tissue of the cyst walls (Figure 9). Chondrocytes and chondrogenesis with ossification were seen in the partially thickened cyst wall (Figure 10).

Statistical analysis

SPSS 22.0 statistical analysis software was used. The measurement data were expressed as Mean±SD. The comparison between different SPECT/CT signs and pathological diagnostic results was analyzed by chi-square test. It was considered statistically different with $p<0.05$.

Results

SPECT/CT imaging results

Features of three-phase bone plane imaging

As shown in Figure 1-3, the soft tissue of the affected ankle joint was higher than that of the healthy side in the perfusion phase, blood pool phase, and delayed phase in 100% (189/189) of patients, and the talus showed abnormal radioactive concentration.

Characteristics of delayed SPECT/CT fusion image

Site of talar cystic lesion: 83% (157/189) of the cystic lesions were located in the medial fornix, 4% (8/189) in the lateral fornix, and 13% (24/189) "symmetrically" distributed in the medial fornix of both ankles.

The extent of cystic lesions in the talus: The extent of cystic lesion involvement was mostly located in the medial fornix of the talus, with the middle anterior 1/3 of the medial fornix being the most common of 27.4% (43/157), anterior to zone 4 of the ninth compartment of Elias (Figure 4). The middle of the medial fornix and the anterior part of the medial fornix were both involved in 27.4% (43/157) of the patients. Larger lesions could extend from the anterior to the posterior part of the medial fornix of the talus in 5.7% (9/157) of the patients. The anterior part was involved separately in 13.4% (21/157) of the patients. The middle part was involved separately in 13.4% (21/157) of the patients. The posterior part was involved separately in 12.7% (20/157) of the patients.

Subarticular facet cystic lesions types: 119 cases of type I (119/189, 63%) and 70 cases of type II (70/189, 37%). The mean CT value of the cystic lesion area: 110 30Hu (80-140Hu), of which the large cyst showed 45 15Hu (30-60Hu) and the small ones showed about 180 40Hu (130-230Hu).

Subchondral bone articular surface continuity: 88% of cases (166/189) showed thicker sclerotic layer of type I cystic lesions, rough subchondral bone articular surface, and faintly visible "chap" like small bone fractures; while almost all (100%) of type II large cystic lesions were connected to the articular surface or connected by narrow channels. In type II, the fractures were more clearly visible than in type I, and in the larger cases, the apical cortical fissures were wider or formed bone defects. Regardless of the size of the cystic lesions, no collapse of the medial talar fornix articular surface was observed. The curvilinear pattern of the talar fornix articular surface remained. The bony articular surface could be worn and thinned.

Hemometabolism of the sclerotic zone: 100% (189/189) of the patients showed a distinctly abnormal concentration of the sclerotic zone around the cystic lesion, which showed a localized high level of hematologic and bone metabolism. The most obvious concentration was located in the anterior part of the talar fornix (the stress point of dorsal extension of the tibial talar joint) in 81% (153/189) of cases. Semi-quantitative analysis: the T/B ratio of the affected talar fornix concentration zone was 2.0 ± 0.5 (range: 1.5-2.5).

Correlation analysis of SPECT/CT features and pathological results

The SPECT/CT imaging of talar cystic lesions showed 88% (166/189 cases) agreement in terms of cystic fractionation, cystic location, and extent of injury involvement, with the intraoperative visual observation and pathologic gross morphology. Twenty-three remained cases did not match, in which the talar dome was no complete exposed intraoperatively or subchondral bone fractures were too small to be visible via CT images.

High CT values (≥ 50Hu) accounted for 27% (19/70) of the cystic lesions, and 89% of cases (17/19) showed mucinous fibroblastic granulation with chondrogenesis and a small amount of osteoid stroma. In two cases, there was a residual bone crest in the cystic lesion. In the low-CT group, only 30% of cases (15 cases) had a small amount of mucinous fibroblastic granulation with chondrogenesis. The remaining 36 cases had only synovial tissue and a small amount of mucus. A significant difference in chondrogenesis was found between these two groups (X^2=20.123，p＜0.001, Table 2).

The T/B ratio in the high uptake area of the talar fornix was larger than 2.0 in 83% (157/189) of cases, with abnormal concentrations at the sclerotic zone around the cystic lesion. One hundred thirty cases showed degeneration of the articular hyaline cartilage matrix with the formation of new bone trabeculae at the edge of the cystic wall. 17% (32/189) of cases had T/B <2.0 in the high uptake area of the talar fornix, with mild sclerosis of the thin cystic wall. The pathological study showed that only 8 cases developed new bone trabeculae, and the difference between the two groups was significant (X^2=45.08，p＜0.001, Table 3).

Discussion

The recognition and treatment of osteochondral injuries of the talus have been controversial worldwide [7-9]. The exact history could hardly be known in most cases, and medical records are rarely documented because early asymptomaticity can be easily overlooked [10]. It has been reported that 25%-50% of patients with ankle sprains will experience chronic, long-term ankle pain for several years after the initial injury (sprain)[11-13]. Therefore, the exact incidence of osteochondral injuries remains unknown, with only one study stating that 27 patients suffered from osteochondral injuries per 100,000 people between 1998 and 2008[14]. Draper et al. found that the incidence of chronic injuries to the talus due to ankle instability was up to 50% [15, 16].

Patients with chronic pain in the ankle joint are common in clinical practice [17]. When the density of the talus is altered on the first radiograph, the attending physician often habitually diagnoses "osteonecrosis of the talus". The terms "osteonecrosis" and "ischemic necrosis" have been used interchangeably in the medical literature for bone death due to impaired circulation [18]. This "necrosis" is often considered to be caused by "circulatory disorder." Thus, osteonecrosis of the talus seems to be a shorthand or synonym for ischemic necrosis of the talus. In contrast, the main clinical causes of ischemic necrosis of the talus are interruption of arterial blood supply and avulsion of the periosteal vascular network of the talar articular surface due to fracture of the talar neck and ankle dislocation. In our cases, there was no history of fracture or dislocation, and the local blood supply, bone metabolism, and pathology of the lesion showed different features from those of ischemic necrosis of the talus.

Three-phase bone imaging shows no ischemia in and around the cystic area of the talus. Compared to the healthy side, the cystic area showed significant concentrations of tracers and abundant blood flow. The blood flow and blood pool phases of the three-phase bone imaging represent the state of blood supply to the lower extremity, especially around the ankle joint, in the arterial and venous phases, respectively. The arterial phase of the affected side is congested, and the dorsalis pedis is patent, without stenosis or occlusion, and slightly more congested than the healthy side. The blood pool image is of the venous phase, with apparent concentrations of tracer at the talus, indicating stasis of blood flow in the venous phase. The static phase, the delayed phase, shows increased subarticular uptake, implying an active bone metabolism that extends over the entire medial (or lateral) aspect of the talus.

Different trauma mechanisms correspond to different injury sites. Some scholars believe that osteochondral injuries of the talus have a typical site of onset, namely the medial fornix or the lateral fornix of the talus, with the medial fornix being particularly common [19-21]. A study at Tong Ren Hospital in China found that the medial middle of the injury accounted for 76% of the injuries [22]. Elias et al. found that the injury located in the medial 1/3 was larger and deeper [3]. Cao et al. noted that deeper position cystic changes in the medial subchondral talus were typical of patients with talar cartilage injuries over 60 years of age [23].

In this study, most of the patients had medial fornix injuries due to dorsal extension and internal rotation. In more severe cases, the posterior part of the medial fornix was involved together, with almost no cases

of posterior involvement alone. In larger cases, the extent of injuries can extend from the anterior to the posterior part of the medial fornix of the talus. We concluded that the cystic lesion began from the anterior to the middle of the medial fornix. The middle and anterior parts were the main areas of involvement. As the disease progresses, it continues to expand anteriorly and posteriorly. Distinguishing from post-fracture talar necrosis, our cases, regardless of size, did not reveal nodal fracture or collapse of the talar fornix. The curvilinear morphology of the articular surface of the talar fornix remained, and the bony articular surface could be phenotypic but never sunken. In contrast, ischemic necrosis of the talar articular surface often shows collapses of the necrotic bone tissue, loss of the normal morphology of the bony articular surface, and compression and flattening of the fornix.

The application of SPECT/CT, a new multimodality imaging method for patients with cystic lesions of the talus, reflects the hemodynamic metabolic status of the osteochondral lesions of the talus in real-time. The subchondral bone cystic lesion and the surrounding area showed the highest active area, and the rest of the talus was a normal physiological bone metabolic zone [24-26]. The sclerotic zone is located at the junction of the lesion area and normal tissue, a zone rich in blood flow, rich in new capillaries, and active in bone metabolism. The location of the obvious concentration of tracers is located in the anterior part of the talar fornix and the stress point of the dorsal extension of the tibial talar joint, where the sclerotic zone is most concentrated, bone metabolism is most active, and blood flow is most abundant.

Simultaneous CT imaging showed alterations in the bone density of the talus. The CT values vary greatly due to the size of the cyst. This is due to the fact that the smaller the cyst, the more it is affected by partial volume. The measurement could introduce significant errors. Around the subchondral bone cystic lesions, calcium salt deposits form unevenly thickened sclerotic bands that form strong mechanical supports, especially in the weight-bearing zone of the tibial talar joint and at mechanical stress points. The sclerotic zone is a compensatory repair and an active response to the injury. The organism manages to protect itself and restore the stability of its mechanical properties while restoring the original bone structure.

Functional imaging of SPECT blood metabolism, CT sclerotic zone morphology, expression of multiple cellular components under pathology comprehensively explained why collapse occurs in femoral head necrosis, but the articular surface of the talar vault does not collapse. It is a weight-bearing joint like the hip and knee, but the talus has a smaller weight-bearing area than the femur and carries almost the entire body's gravity. It is subject to more stress than the knee and hip and is more likely to cause injury. Our SPECT/CT study confirmed that the blood supply to the affected limb was increased, and the ankle joint was rich in blood circulation and active in bone metabolism.

The pathology showed the following features consistent with SPECT/CT findings in the large cysts: 1, tortuous fibrocystic wall; 2, numerous dense fibroblast proliferation and abundant collagen fibers; 3, granulation tissue and inflammatory cell aggregation around the cyst wall; 4, chondrogenesis with ossification, and active osteogenesis around the necrotic lesion. The pathologically active chondrogenesis and ossification explain the abnormal concentration of tracers in the cystic cavity on

SPECT/CT static fusion images. The presence of osteogenic repair activity within the cystic lesion is secondary to the injury. Focal necrosis of the talar injury occurred in conjunction with a marked congestive and inflammatory response, active fibrous and bone repair, and rapid formation of a sclerotic shell of protective new bone around the cystic lesion. It maintained the overall integrity and normal morphology of the articular surface of the talus under considerable stress. This is in contrast to the deformation of the femoral head caused by massive osteonecrosis in aseptic femoral head necrosis. However, there are still many questions about the definite cause of cystic degeneration after talar injury and the process of its own repair. This will be the direction of our further research. At present, it is still the best clinical treatment option, minimally invasive means with bone grafting, to revascularize and provide osteoinduction and osteoconduction[27, 28], and to enhance local support and improve ankle stability.

The causes of OLT formation are a popular issue of interest to many scholars, and the causes may be multifaceted. Cystic lesions are associated with trauma and are part of osteochondral damage. Continuous small cystic lesion formation is distributed over the joint surface and occurs where the most force is exerted. When the external forces are less than the shear forces that the cartilage can withstand and greater than the subchondral bone, a fracture or microfracture of the subchondral bone will happen in the presence of cartilage. Besides, the local microenvironment is altered, resulting in a focal necrotic capsular lesion. It differs from ischemic necrosis in that the talus is rich in blood flow and activity in osteogenesis, allowing for immediate repair and reconstruction. For treatment, minimally invasive surgery that takes full advantage of this and performs drilling combined with bone grafting is the recommended method. In conclusion, SPECT/CT three-phase bone imaging is advantageous in identifying the cause of talar injury, while SPECT/CT delayed imaging is advantageous in observing the location, extent of involvement, classification, and repair of cystic lesions in the talus.

Abbreviations

OLT: Osteochondral lesions of the talus; CT: Computed tomography

Declarations

Acknowledgements

We would like to thank the person who gave assistance to this study.

Funding

Not applicable.

Availability of data and materials

The datasets generated and/or analyzed during the current study are not available based on the protection of patient privacy, but are available from the corresponding author on reasonable request.

Authors' contributions

QTS and XLM contributed to the design of the study. QTS drafted the manuscript with the help from XTZ, HJH, JX and LL. XTZ and HJH helped in the statistical analyses. Statistical analyses were discussed with LL and SSC. QTS, ZHL and XLM contributed to the revision. All authors have read and approved the final manuscript.

Competing interest

The authors declare that they have no competing interests.

Ethics approval and consent to participate

This research was approved by the ethics committee of Tianjin Hospital and performed in accordance with the Declaration of Heisinki. And agreement to participate was given by the participants. Informed written consent was obtained from all participants.

Consent for publication

Not applicable.

References

[1] Berndt AL, Harty MJJ. Transchondral fractures (osteochondritis dissecans) of the talus. 1959;41:1363.

[2] Loomer R, Fisher C, Lloyd-Smith R, Sisler J, Cooney T. Osteochondral lesions of the talus. Am J Sports Med. 1993;21:13-9.

[3] Raikin SM, Elias I, Zoga AC, Morrison WB, Besser MP, Schweitzer MEJF, et al. Osteochondral lesions of the talus: localization and morphologic data from 424 patients using a novel anatomical grid scheme. 2007;28:154-61.

[4] Nakasa T, Ikuta Y, Yoshikawa M, Sawa M, Tsuyuguchi Y, Adachi NJTAjosm. Added value of preoperative computed tomography for determining cartilage degeneration in patients with osteochondral lesions of the talar dome. 2018;46:208-16.

[5] Teramoto A, Shoji H, Kura H, Sakakibara Y, Kamiya T, Watanabe K, et al. Investigation of factors related to the occurrence of osteochondral lesions of the talus by 3D bone morphology of the ankle. 2018;100:1487-90.

[6] Deng E, Gao L, Shi W, Xie X, Jiang Y, Yuan H, et al. Both Magnetic Resonance Imaging and Computed Tomography Are Reliable and Valid in Evaluating Cystic Osteochondral Lesions of the Talus. 2020;8:2325967120946697.

[7] Seo SG, Kim JS, Seo DK, Kim YK, Lee SH, Lee HS. Osteochondral lesions of the talus. Acta Orthop. 2018;89:462-7.

[8] Nakasa T, Ikuta Y, Sawa M, Yoshikawa M, Tsuyuguchi Y, Ota Y, et al. Evaluation of Articular Cartilage Injury Using Computed Tomography With Axial Traction in the Ankle Joint. Foot Ankle Int. 2018;39:1120-7.

[9] Posadzy M, Desimpel J, Vanhoenacker F. Staging of Osteochondral Lesions of the Talus: MRI and Cone Beam CT. J Belg Soc Radiol. 2017;101.

[10] Hamilton C, Burgul R, Kourkounis G, Howieson A, Papadopoulos AJTF. Osteochondral defects of the talus: radiological appearance and surgical candidate profiling—A retrospective analysis. 2021;46:101767.

[11] DiGiovanni BF, Partal G, Baumhauer JF. Acute ankle injury and chronic lateral instability in the athlete. Clin Sport Med. 2004;23:1-+.

[12] Anandacoomarasamy A, Barnsley L. Long term outcomes of inversion ankle injuries. Brit J Sport Med. 2005;39.

[13] Fong DTP, Hong YL, Chan LK, Yung PSH, Chan KM. A systematic review on ankle injury and ankle sprain in sports. Sports Med. 2007;37:73-94.

[14] Orr JD, Dawson LK, Garcia EJ, Kirk KL. Incidence of Osteochondral Lesions of the Talus in the United States Military. Foot Ankle Int. 2011;32:948-54.

[15] Draper SD, Fallat LM. Autogenous bone grafting for the treatment of talar dome lesions. J Foot Ankle Surg. 2000;39:15-23.

[16] Ferkel RD, Chams RN. Chronic lateral instability: arthroscopic findings and long-term results. Foot Ankle Int. 2007;28:24-31.

[17] Nakasa T, Ikuta Y, Sawa M, Yoshikawa M, Tsuyuguchi Y, Ota Y, et al. Relationship Between Bone Marrow Lesions on MRI and Cartilage Degeneration in Osteochondral Lesions of the Talar Dome. Foot Ankle Int. 2018;39:908-15.

[18] Talusan PG, Milewski MD, Toy JO, Wall EJ. Osteochondritis Dissecans of the Talus: Diagnosis and Treatment in Athletes. Clin Sport Med. 2014;33:267-+.

[19] Maceira E, Monteagudo M. Subtalar Anatomy and Mechanics. Foot Ankle Clin. 2015;20:195-+.

[20] Walley KC, Gonzalez TA, Callahan R, Fairfull A, Roush E, Saloky KL, et al. The Role of 3D Reconstruction True-Volume Analysis in Osteochondral Lesions of the Talus: A Case Series. Foot Ankle Int. 2018;39:1113-9.

[21] King JL, Walley KC, Stauch C, Bifano S, Juliano P, Aynardi MCJF, et al. Comparing the Efficacy of True-Volume Analysis Using Magnetic Resonance Imaging With Computerized Tomography and Conventional Methods of Evaluation in Cystic Osteochondral Lesions of the Talus: A Pilot Study. 2020:1938640020928177.

[22] Hao DP, Zhang JZ, Wang ZC, Xu WJ, Liu JH, Yang BT. Osteochondral Lesions of the Talus Comparison of Three-Dimensional Fat-Suppressed Fast Spoiled Gradient-Echo Magnetic Resonance Imaging and Conventional Magnetic Resonance Imaging. J Am Podiat Med Assn. 2010;100:189-94.

[23] Cao YX, Xu Y, Huang Q, Hong Y, Xu XY. Characteristics of Osteochondral Lesions of the Talus in Different Age Groups. Int J Sports Med. 2020;41:873-8.

[24] Pelletier-Galarneau M, Martineau P, Gaudreault M, Pham X. Review of running injuries of the foot and ankle: clinical presentation and SPECT-CT imaging patterns. Am J Nucl Med Mol Imaging. 2015;5:305-16.

[25] Liu H, Guo H, Guo S, Wang J, Ye Y, Ma C. Novel treatment of 99Tc-MDP improves clinical and radiographic results for patients with osteochondral lesions of the talus. Q J Nucl Med Mol Imaging. 2019;63:199-206.

[26] Hassink G, Testa EA, Leumann A, Hugle T, Rasch H, Hirschmann MT. Intra- and inter-observer reliability of a new standardized diagnostic method using SPECT/CT in patients with osteochondral lesions of the ankle joint. Bmc Med Imaging. 2016;16.

[27] Leumann A, Horisberger M, Buettner O, Mueller-Gerbl M, Valderrabano V. Medial malleolar osteotomy for the treatment of talar osteochondral lesions: anatomical and morbidity considerations. Knee Surg Sport Tr A. 2016;24:2133-9.

[28] Slullitel PAI, Tripodi ML, Bosio ST, Puigdevall M, Maenza R. Massive Osteochondral Lesion of the Talus in a Skeletally Immature Patient Associated With a Tarsal Coalition and Valgus Hindfoot. Journal of Foot & Ankle Surgery. 2017;56:1257-62.

Tables

Table 1 Summary of demographic data in 189 patients

Variable	n（%）
Gender (male:female)	2.5:1
Age	
20-30	15（8%）
31-40	67（35%）
41-50	62（34%）
51-60	31（16%）
＞60	14（7%）
Medical history	
Ankle internal rotation	161（85%）
Ankle movement restricted	28（15%）
Clinical symptoms	
Mild swelling of the ankle	42（22%）
Medial ankle pain	168（89%）

Table 2 Correlation analysis of CT values of the talar cystic area with pathological chondrogenesis

CT value	Chondrogenesis (-)	Chondrogenesis (+)	c^2	*P*
＜50Hu	36	15	20.123	0.000
≥50Hu	2	17		

Table 3 Correlation analysis of T/B ratio with pathological new bone trabeculae at high uptake area

New bone trabeculae	T/B＜2.0	T/B≥2.0	c^2	*P*
Negative	24	27	45.077	0.000
Positive	8	130		

T/B is the ratio of the radioactivity of the affected side to the healthy side in the high uptake area of the talar dome.

Figures

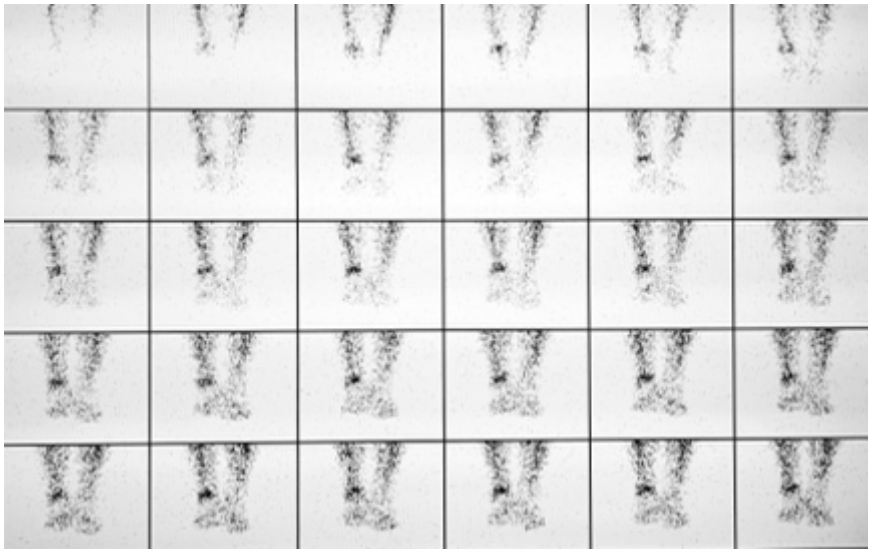

Figure 1

Blood flow in the larger artery of the lower leg. The tracer concentration on the affected side is higher than that on the healthy side, suggesting that the lower leg on the affected side is congested.

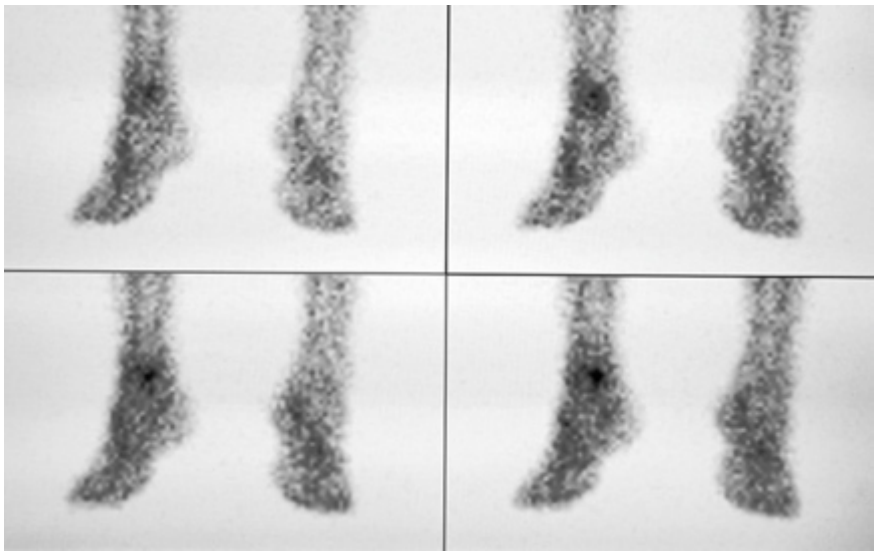

Figure 2

Blood pool phase: dotted tracer concentration is visible on the affected ankle, and the overall tracer concentration on the affected side is enhanced compared to the healthy side, showing a bruised state.

Figure 3

Delayed phase (static phase): punctate tracer concentration in the affected ankle joint. It suggests active local bone metabolism.

Figure 4

Hand drawing of the Elias subdivision of the talar dome: the distribution of this group of lesions are mainly concentrated in the medial mid-anterior part.

Figure 5

Male, 57 years old, with left ankle pain for more than five years, history of the minor sprain, and other medical histories. CT sagittal (a) and coronal (c) images show multiple consecutive small bursae with sclerosis of the surrounding bone visible in the subchondral bone of the talar fornix. This is consistent with a type I cystic lesion. SPECT/CT fusion images (b,d) show that the area of tracer concentration in the talar fornix corresponds to the cystic area and the surrounding sclerotic bone.

Figure 6

Male, 65 years old, had left ankle pain for 4.5 years, aggravated for one week. The fusion image showed that the lateral fornix of the left talus was locally fractured and the articular surface was not smooth, and multiple small capsular hypodense shadows were seen underneath it with obvious sclerosis of the edges. A larger cystic hypointense shadow was seen below the anterior part of the small cyst, and a narrow channel could be seen connecting with the articular surface, and the local bone cortex was not continuous. The area of anomalous tracer concentration in the left talus corresponds to the area of foraminal cystic degeneration. (Type II cystic lesion) (a) Sagittal type II large cyst formation; (b) large cyst communicating with the articular surface; (c) multiple small cysts in axial position. (d) SPECT/CT fusion image

Figure 7

Gross specimen with subchondral bone defect and mucus-like material residue visible at the cystic lesion.

Figure 8

HE100×, Part of the bone traps were empty, osteocytes disappeared, fibroblasts proliferated, and collagen fibers were abundant, inflammatory cells were gathered, and fibroblastic granulation tissue grew in between the necrotic bone trabeculae.

Figure 9

The Scattered bone-like stroma is visible between the hyperplastic granulation tissue of the HE100× tortuous fibrous cyst wall.

Figure 10

HE100×, Chondrocytes, and chondrogenesis with ossification are visible in the thickened cyst wall.